

Gravitational Waves of Holographic QCD Phase Transition with Hyperscaling Violation

Zhourun Zhu ¹, Manman Sun ¹, Rui Zhou ¹, Jinzhong Han ¹ and Defu Hou ^{2,*} 

¹ School of Physics and Telecommunications Engineering, Zhoukou Normal University, Zhoukou 466001, China; zhuzhourun@zknknu.edu.cn (Z.Z.); sunmm@zknknu.edu.cn (M.S.); ruychou@zknknu.edu.cn (R.Z.); hanjinzhong@zknknu.edu.cn (J.H.)

² Institute of Particle Physics and Key Laboratory of Quark and Lepton Physics (MOS), Central China Normal University, Wuhan 430079, China

* Correspondence: houdf@mail.cnu.edu.cn

Abstract: In this paper, we study the gravitational waves of holographic QCD phase transition with hyperscaling violation. We consider an Einstein–Maxwell Dilaton background and discuss the confinement–deconfinement phase transition between thermally charged AdS and AdS black holes. We find that hyperscaling violation reduces the phase transition temperature. In a further study, we discuss the effect of hyperscaling violation on the GW spectrum. We found that the hyperscaling violation exponent suppresses the peak frequency of the total GW spectrum. Moreover, the results of the GW spectrum may be detected by IPTA, SKA, BBO, and NANOGrav. We also find that the hyperscaling violation exponent suppresses the peak frequency of the bubble-collision spectrum $h^2\Omega_{env}$. Hyperscaling violation enhances the energy densities of the sound wave spectrum $h^2\Omega_{sw}$ and the MHD turbulence spectrum $h^2\Omega_{turb}$. The total GW spectrum is dominated by the contribution of the bubble collision in runaway bubbles case.

Keywords: AdS/CFT correspondence; QCD phase transition; gravitational waves; cosmology



Citation: Zhu, Z.; Sun, M.; Zhou, R.; Han, J.; Hou, D. Gravitational Waves of Holographic QCD Phase Transition with Hyperscaling Violation. *Universe* **2024**, *10*, 224. <https://doi.org/10.3390/universe10050224>

Academic Editor: Lorenzo Iorio

Received: 10 April 2024

Revised: 14 May 2024

Accepted: 15 May 2024

Published: 17 May 2024



Copyright: © 2024 by the authors. Licensee MDPI, Basel, Switzerland. This article is an open access article distributed under the terms and conditions of the Creative Commons Attribution (CC BY) license (<https://creativecommons.org/licenses/by/4.0/>).

1. Introduction

Albert Einstein’s prediction based on the principles of general relativity suggests that gravitational waves (GWs) manifest as perturbations in the curvature of spacetime [1,2]. The relic of gravitational waves carries crucial information about the nature of its source, which can be deciphered. The detection of the GW signal at the Laser Interferometer Gravitational Wave Observer (LIGO) [3] has offered a new approach to exploring astronomy and cosmology. Recently, the North American NanoHertz Observatory for Gravitational Waves (NANOGrav) [4] reported a stochastic process that could potentially be interpreted as a significant signal of stochastic gravitational waves. This indicative evidence is derived from a comprehensive analysis of 12.5-year pulsar timing array data.

The sources of gravitational waves can originate from astrophysical or cosmological phenomena [5]. Phase transitions (PTs) are a usual phenomenon in cosmological origins. When the temperature decreased, the universe may have undergone several PTs. When the first-order phase transition happens, two free-energy local minima coexist within a certain temperature range. The relevant scalar field has the potential to undergo quantum tunneling or thermal fluctuations, which leads to a transition into the new phase. Quantum or thermal processes occur through the nucleation of bubbles in the broken phase. The bubbles subsequently undergo expansion and ultimately collide with each other. This process is highly violent and non-uniform, which may lead the generation of the gravitational waves [6–13].

QCD phase transitions occur when the temperature is several hundred MeV. In order to investigate the QCD phase structure, scientists carry out heavy-ion-collision experiments at RHIC and LHC [14–16]. It is believed that hconfinement–deconfinement QCD phase

transitions occur and that QGP is formed in experiments. Lattice QCD results reveal that the QCD phase transition is first-order when considering heavy, static quarks or pure gauge theory [17]. When physical quark masses are taken into account, PT becomes a crossover [18–20]. Exploring QCD phase transition helps us comprehend the evolution of the universe.

AdS/CFT correspondence [21–23] provides a different perspective to study gravitational waves of first-order QCD phase transitions. From a holographic perspective, the confinement–deconfinement phase transition is dual with respect to the Hawking–Page phase transition [24]. The Hawking–Page PT in soft-wall and hard-wall models has been investigated in [25]. Inspired by [25], the authors of [26] discuss gravitational waves of first-order QCD phase transition in AdS/QCD. In [27], the authors discuss the phase transition with finite chemical potential and study the GWs with different bubble wall velocities. The effect of finite coupling on the GW spectrum has been studied in [28,29]. The GWs of QCD phase transition in holographic EMD models have been discussed in [30–33]. The GWs of QCD phase transition with gluon condensate has been studied in [34]. Other significant work can be seen in [35,36].

Researchers consider the generalized geometries to not be asymptotically AdS. These geometries do not possess conformal invariance in dual field theories but still exhibit scale invariance. One important example is Lifshitz geometry and Lifshitz fixed point displays anisotropic scale symmetry [37,38]. One of the metrics of Lifshitz geometry in Euclidean signatures can be given by [39]

$$ds^2 = r^{2\alpha} \left(r^{2z} dt^2 + \frac{1}{r^2} dr^2 + r^2 \sum_{i=1}^d dx_i^2 \right), \quad \alpha = -\theta/d, \quad (1)$$

where θ denotes the hyperscaling violation exponent, z is the dynamical exponent, and d represents the spatial dimension. In such metrics, conformal invariance is directly violated, making it pertinent to investigate the nature of quantum chromodynamics (QCD) [40]. The metric (1) is spatially homogeneous and covariant because it uses the scale transformations, $t \rightarrow \lambda^z, r \rightarrow \lambda^{-1}r, x_i \rightarrow \lambda x_i, ds_{d+2}^2 \rightarrow \lambda^{\theta/d} ds_{d+2}^2$. The background is scaled anisotropically and spatially isotropic when $z \neq 1$. The distance is not invariant when $\theta \neq 0$, which refers to the hyperscaling violations in dual field theory. Other hyperscaling violating Lifshitz models can be seen in [41–44].

In this paper, we consider an Einstein–Maxwell dilaton background with nonzero hyperscaling violation and chemical potential. We study the Hawking–Page PT between thermally charged AdS and AdS black holes. We discuss the effect of hyperscaling violation and chemical potential on phase transition temperatures. One of sources of GW signals is cosmological first-order PTs. Then, we study the effect of hyperscaling violation on GWs and compare it with the detection results of the International Pulsar Timing Array (IPTA), Square Kilometer Array (SKA), Big Bang Observer (BBO) [45], TianQin, Taiji [46,47], and the North American NanoHertz Observatory for Gravitational Waves (NANOGrav) [4].

The paper is organized as follows. In Section 2, we discuss the effect of hyperscaling violation and chemical potential on phase transition. In Section 3, we study the gravitational waves of the QCD phase transition with hyperscaling violation. The conclusion and discussion are given in Section 4.

2. Holographic QCD Phase Transition with Hyperscaling Violation

In this section, we will study the effect of hyperscaling violation and chemical potential on confinement–deconfinement phase transitions in an Einstein–Maxwell dilaton background. We first review the work of [40]. The author of [40] calculates the free energy difference and studies the QCD phase transition with hyperscaling violation. The gravity action with a dilaton field is given by [44]

$$S = - \int d^{d+2}x \sqrt{g} \left[\frac{1}{2k^2} (R - \frac{1}{2} (\partial\phi)^2 + V_0 e^{\gamma\phi}) - \frac{1}{4g^2} F^2 e^{\lambda\phi} \right], \quad (2)$$

where $1/2k^2 = N_c^2/8\pi^2$ and $1/2g^2 = N_c N_f/8\pi^2$ [48]. N_c and N_f are the numbers of color and flavor, respectively. d is the dimension. λ , γ , and V_0 are parameters of this model. In this work, we set the dynamical exponent $z = 1$.

The ansatz of metric is [44]

$$ds^2 = r^{2\alpha} \left(r^2 f(r) dt^2 + \frac{1}{r^2 f(r)} dr^2 + r^2 \sum_{i=1}^d dx_i^2 \right), \quad \phi = \phi(r), \tag{3}$$

where the dilaton field is given by $e^\phi = e^{\phi_0} r^{\sqrt{2d\alpha(\alpha+1)}}$. Then, we can find $\alpha(\alpha + 1)$, which must be larger than zero, and the solutions are well defined in this case.

In order to discuss the QCD phase transition with hyperscaling violation, we should obtain the solutions of the blackening function in the black hole phase and the thermally AdS phase. The deconfinement phase with hyperscaling violation and chemical potential is dual to the charged AdS black hole with hyperscaling violation. The blackening function $f(r)$ of a charged AdS black hole is given by

$$f(r) = 1 - \frac{m}{r^{d(1+\alpha)+1}} + \frac{Q^2}{r^{2d(1+\alpha)}}, \tag{4}$$

where m and Q denote the black hole mass and charge, respectively. The black hole mass can be obtained by $f(r_h) = 0$.

The field strength is

$$F_{rt} = i\bar{Q}r^{-d(\alpha+1)}, \tag{5}$$

where $\bar{Q} = \frac{g}{k} \sqrt{d(1+\alpha)(d\alpha+d-1)} e^{-\lambda\phi_0/2}$ [40].

The time component of the bulk gauge field $A_t(r)$ is

$$A_t(r) = i \left(\mu - \frac{\bar{Q}}{d(\alpha+1)-1} r^{-d(\alpha+1)+1} \right). \tag{6}$$

The gauge field is equal to zero when $r = r_h$. Then, we can obtain the relation between the chemical potential μ and \bar{Q} :

$$\bar{Q} = \frac{d(\alpha+1)-1}{r_h^{-d(\alpha+1)+1}} \mu, \Rightarrow Q = \frac{k}{g} \mu \sqrt{\frac{d(\alpha+1)-1}{d(\alpha+1)}} e^{\lambda\phi_0/2} r_h^{d(\alpha+1)-1}. \tag{7}$$

The Hawking temperature of a black hole is [40]

$$T = \frac{1}{4\pi} (d\alpha + d + 1) r_h \left(1 - \mu^2 \frac{k^2}{g^2} \frac{(d\alpha + d - 1)^2}{d(1+\alpha)(d\alpha + d + 1)} e^{\lambda\phi_0} \frac{1}{r_h^2} \right). \tag{8}$$

The regularized action of the AdS black hole is calculated as

$$S_{BH} = -V_d \beta_{BH} \frac{1+\alpha}{k^2} (r_h^{d(\alpha+1)+1} + Q^2 r_h^{-d(\alpha+1)+1}), \tag{9}$$

where β_{BH} is inverse of temperature and V_d is the d-dimensional volume.

Using thermodynamical relation $F = TS/V_d$, one can obtain the free energy density F of the black hole

$$F_{BH} = -\frac{1+\alpha}{k^2} (r_h^{d(\alpha+1)+1} + Q^2 r_h^{-d(\alpha+1)+1}). \tag{10}$$

In order to calculate the free energy density differences, we should obtain the free energy density of thermally charged AdS. Thermally charged AdS is dual to the confinement

phase and does not exist horizon [49]. The blackening function $f_1(r)$ of a thermally charged AdS with hyperscaling violation is [40]

$$f_1(r) = 1 + \frac{Q_1^2}{r^{2d(\alpha+1)}}, \tag{11}$$

where $Q_1 = \frac{k}{2g} \mu \sqrt{\frac{d(\alpha+1)-1}{d(\alpha+1)}} e^{\lambda\phi_0/2} r_{IR}^{d(\alpha+1)-1}$ is the charge of thermally charged AdS and r_{IR} is the cut-off.

The field strength and gauge field of a thermally charged AdS are

$$F_{1rt} = i\overline{Q_1} r^{-d(\alpha+1)}, \quad A_{1t}(r) = \frac{i\overline{Q_1}}{1-d(\alpha+1)} r^{-d(\alpha+1)+1} + C_2, \tag{12}$$

where $\overline{Q_1} = \frac{g}{k} Q_1 \sqrt{d(\alpha+1)(d\alpha+d-1)} e^{-\lambda\phi_0/2}$ and $C_2 = A_{1t}(\infty) = i\mu$.

The regularized action of a thermally charged AdS is

$$S_{tc} = -V_d \beta_1 \frac{1+\alpha}{k^2} (r_{IR}^{d(\alpha+1)+1} + Q_1^2 r_{IR}^{-d(\alpha+1)+1}), \tag{13}$$

where β_1 is the period.

Using the thermodynamical relation $F = TS/V_d$, one can obtain the free energy density of the thermally charged AdS:

$$F_{tc} = -\frac{1+\alpha}{k^2} (r_{IR}^{d(\alpha+1)+1} + Q_1^2 r_{IR}^{-d(\alpha+1)+1}). \tag{14}$$

The free energy density differences can be obtained from Equations (10) and (14) [40]:

$$\Delta F = \frac{1}{k^2} \left[(r_{IR}^{d(\alpha+1)+1} - r_h^{d(\alpha+1)+1}) + \mu^2 (d(1+\alpha) - 1) e^{\lambda\phi_0} \left(\frac{1}{4} r_{IR}^{d(\alpha+1)-1} - r_h^{d(\alpha+1)-1} \right) \right]. \tag{15}$$

The confinement–deconfinement phase transition happens when the free energy density difference $\Delta F = 0$. By using Equation (15), we can calculate the phase transition temperature with nonzero chemical potential and hyperscaling violation. In the numerical calculation, we take $r_{IR} = 323$ MeV, which is related to the mass of the lightest ρ mesons [25]. As for other parameters, we take $N_c = 3, N_f = 2, d = 3$ and $\phi_0 = 0$.

We analyze the results and plot the figures by using the software Mathematica. The codes of Mathematica that we used are mainly partial derivative, solve, numerical calculations, ListLinePlot, and LogLogPlot. The partial derivative, solve and numerical calculation codes are used to obtain the numerical values. The ListLinePlot and LogLogPlot codes are used to plot figures.

When the values of chemical potential, hyperscaling violation, and other parameters are fixed, one can set $\Delta F = 0$ to obtain the results of r_h . Then, one can plug the values of r_h into the Hawking temperature, Equation (8), and one can obtain the phase transition temperature. We plot the figures using Mathematica.

In Figure 1, we present the effect of hyperscaling violation on the phase transition temperature. This plot shows a direct correlation between the phase transition temperature and the parameter α : as α increases, so does the phase transition temperature. Also, α is negatively correlated with hyperscaling violation exponent θ from Equation (1), implying that an increase in α corresponds to a decrease in hyperscaling violation. Additionally, we observe that as the chemical potential increases, the phase transition temperature decreases, which is consistent with the results of [40].

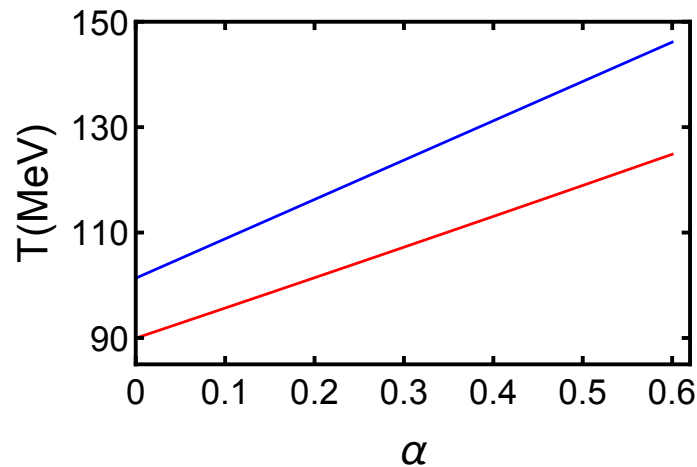


Figure 1. The effect of hyperscaling violation on phase transition temperature. The blue line represents $\mu = 0.05$ GeV, and the red line represents $\mu = 0.15$ GeV.

3. Gravitational Waves from Holographic QCD Phase Transition with Hyperscaling Violation

In this section, we discuss the GWs from the holographic confinement–deconfinement phase transition with hyperscaling violation. First-order PTs can be regarded as one of the sources of GWs. When a first-order PT happens, the bubbles nucleate and expand. Bubbles ultimately collide with each other and contribute to the production of GWs. Furthermore, sound waves and magnetohydrodynamic (MHD) turbulence also favor the generation of GWs. Thus, the total GW spectrum ($h^2\Omega(f)$) includes bubble collisions ($h^2\Omega_{env}$), sound waves ($h^2\Omega_{sw}$), and MHD turbulence ($h^2\Omega_{turb}$). $h^2\Omega(f)$ can be given by [9]

$$h^2\Omega(f) = h^2\Omega_{env}(f) + h^2\Omega_{sw}(f) + h^2\Omega_{turb}(f), \tag{16}$$

where

$$\begin{aligned} h^2\Omega_{env}(f) &= 1.67 \times 10^{-5} \left(\frac{0.11v_b^3}{0.42 + v_b^2} \right) \left(\frac{H_*}{\tau} \right)^2 \left(\frac{\kappa\gamma}{1 + \gamma} \right)^2 \left(\frac{100}{g_*} \right)^{\frac{1}{3}} S_{env}(f), \\ h^2\Omega_{sw}(f) &= 2.65 \times 10^{-6} \left(\frac{H_*}{\tau} \right) \left(\frac{\kappa_v\gamma}{1 + \gamma} \right)^2 \left(\frac{100}{g_*} \right)^{\frac{1}{3}} v_b S_{sw}(f), \\ h^2\Omega_{turb}(f) &= 3.35 \times 10^{-4} \left(\frac{H_*}{\tau} \right) \left(\frac{\kappa_{turb}\gamma}{1 + \gamma} \right)^{\frac{3}{2}} \left(\frac{100}{g_*} \right)^{\frac{1}{3}} v_b S_{turb}(f). \end{aligned} \tag{17}$$

The GW spectral shapes are

$$\begin{aligned} S_{env}(f) &= \frac{3.8 \left(\frac{f}{f_{env}} \right)^{2.8}}{1 + 2.8 \left(\frac{f}{f_{env}} \right)^{3.8}}, \\ S_{sw}(f) &= \left(\frac{f}{f_{sw}} \right)^3 \left(\frac{7}{4 + 3 \left(\frac{f}{f_{sw}} \right)^2} \right)^{\frac{7}{2}}, \\ S_{turb}(f) &= \frac{\left(\frac{f}{f_{turb}} \right)^3}{\left(1 + \frac{f}{f_{turb}} \right)^{\frac{11}{3}} \left(1 + \frac{8\pi f}{h_*} \right)}, \end{aligned} \tag{18}$$

with

$$h_* = 16.5 \times 10^{-6} [\text{Hz}] \left(\frac{T_*}{100 \text{ GeV}} \right) \left(\frac{g_*}{100} \right)^{\frac{1}{6}}. \tag{19}$$

The peak frequencies are

$$\begin{aligned} f_{env} &= 16.5 \times 10^{-6} [\text{Hz}] \left(\frac{f_*}{\tau} \right) \left(\frac{\tau}{H_*} \right) \left(\frac{T_*}{100 \text{ GeV}} \right) \left(\frac{g_*}{100} \right)^{\frac{1}{6}}, \\ f_{sw} &= 1.9 \times 10^{-5} [\text{Hz}] \left(\frac{1}{v_b} \right) \left(\frac{\tau}{H_*} \right) \left(\frac{T_*}{100 \text{ GeV}} \right) \left(\frac{g_*}{100} \right)^{\frac{1}{6}}, \\ f_{turb} &= 2.7 \times 10^{-5} [\text{Hz}] \left(\frac{1}{v_b} \right) \left(\frac{\tau}{H_*} \right) \left(\frac{T_*}{100 \text{ GeV}} \right) \left(\frac{g_*}{100} \right)^{\frac{1}{6}}, \end{aligned} \tag{20}$$

where

$$\frac{f_*}{\tau} = \frac{0.62}{1.8 - 0.1v_b + v_b^2}. \tag{21}$$

The parameters can be obtained by

$$\kappa = 1 - \frac{\gamma_\infty}{\gamma}, \quad \kappa_v = \frac{\gamma_\infty}{\gamma} \frac{\gamma_\infty}{0.73 + 0.083\sqrt{\gamma_\infty + \gamma_\infty}}, \quad \kappa_{tu} = \epsilon \kappa_v, \tag{22}$$

where κ is the efficiency factor in bubble collision, κ_v denotes the fraction or proportion that is converted into fluid motion, and κ_{tu} represents the contribution of MHD turbulence. The value of ϵ is 0.05–0.1 [50] and represents the proportion of bulk motion which is turbulent. In the following calculations, we set $\epsilon = 0.05$. τ^{-1} is the phase transition duration. H_* denotes the Hubble parameter at the phase transition temperature. Here, we take $\tau/H_* = 10$.

The parameter γ represents the ratio of vacuum energy density to radiation energy density. γ_∞ denotes the minimum value of γ . The expressions of these parameters are

$$\gamma = \frac{\epsilon_*}{\frac{\pi^2}{30} g_* T_*^4}, \quad \gamma_\infty = \frac{30}{24\pi^2} \frac{\sum_a c_a \Delta m_a^2}{g_* T_*^2}. \tag{23}$$

where T_* denotes the phase transition temperature, and g_* represents the number of effective relativistic degrees of freedom. As discussed in [26,27], we set $T_* \simeq T_c$ and $g_* \sim 10$ in the calculations. c_a is equal to $N_a(\frac{1}{2}N_a)$ for boson (fermion) species, Δm_a is the particle mass difference, we take $\Delta m_a \sim 500$ MeV [51], and ϵ_* represents the vacuum energy:

$$\epsilon_* = \left(-\Delta F(T) + T \frac{d\Delta F(T)}{dT} \right) \Big|_{T=T_*}. \tag{24}$$

The bubble wall speed v_b can reach the light speed [52] in the case of $\gamma > \gamma_\infty$ case (runaway bubbles), namely $v_b = 1$. The total GW pectrum can be denoted as $h^2\Omega(f) = h^2\Omega_{env}(f) + h^2\Omega_{sw}(f) + h^2\Omega_{turb}(f)$. In the $\gamma < \gamma_\infty$ case, the contribution of bubble collision can be negligible. Thus, $h^2\Omega(f) = h^2\Omega_{sw}(f) + h^2\Omega_{turb}(f)$.

From the results of Equation (15), one can calculate the vacuum energy ϵ_* of Equation (24). Then, the values of γ and γ_∞ can be obtained by Equation (23). It is found that $\gamma > \gamma_\infty$ from numerical calculations in this model; thus, we will discuss the effect of hyperscaling violation on GW spectrum in the case of runaway bubbles. Next, we calculate the values of κ , κ_v , and κ_{tu} from Equation (22). Finally, one can plot the GW spectrum from Equations (16) and (17).

In Figure 2, we plot the total GW spectrum produced from the first-order QCD phase transition with hyperscaling violation when $\mu = 0.05$ GeV. This figure shows a direct correlation between the peak frequency and the parameter α : as α increases, the position of peak frequency moves forward. α is negatively correlated to the hyperscaling violation exponent θ . Thus, the peak frequency is suppressed by hyperscaling violation θ . Moreover,

the resulting GW spectrum can be detected by IPTA, SKA, and BBO [45]. To be specific, the GW spectrum can be detected by IPTA and SKA in the 1×10^{-9} – 1×10^{-7} Hz region. The GW spectrum may be detected by BBO around 1×10^{-1} Hz. The GW spectrum may be detected by NANOGrav [4] around 1×10^{-8} Hz at a large hyperscaling violation θ (small α). The GW signals can not be probed by TianQin and Taiji [46,47] temporarily.

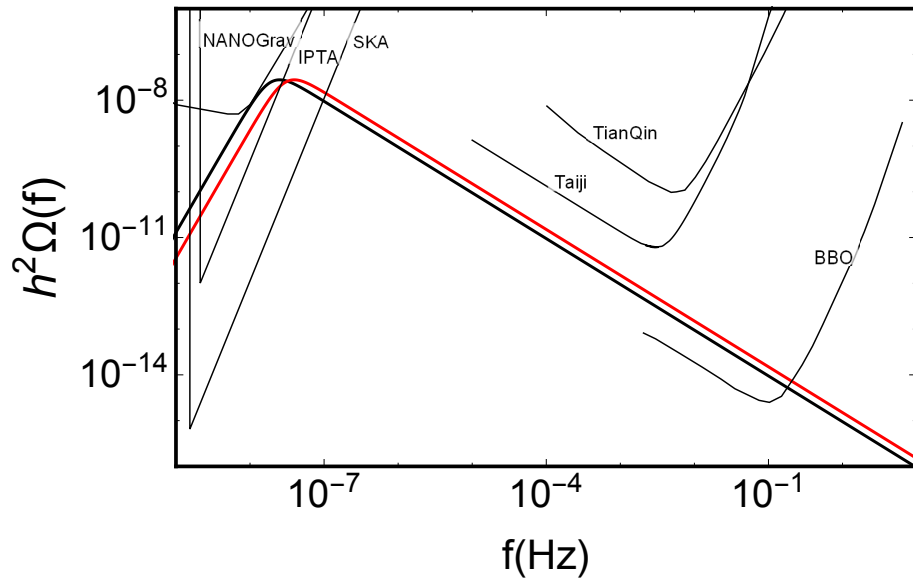


Figure 2. The GW spectrum produced from the first-order QCD phase transition with hyperscaling violation when $\mu = 0.05$ GeV. The black line represents $\alpha = 0.01$, and the red line represents $\alpha = 0.7$.

In Figure 3, we plot the effect of hyperscaling violation on the spectrum of bubble collision ($h^2\Omega_{env}$), sound waves ($h^2\Omega_{sw}$), and magnetohydrodynamic turbulence ($h^2\Omega_{turb}$) in (a), (b), and (c), respectively. We discuss the contribution of bubble collision, sound waves, and magnetohydrodynamic turbulence on the total GW spectrum ($h^2\Omega(f)$) in (d). From Figure 3a, we can observe that the position of peak frequency of $h^2\Omega_{env}$ moves forward when increasing the parameter α . Thus hyperscaling violation θ suppresses the peak frequency of $h^2\Omega_{env}$. From Figure 3b,c, we can find that the energy densities of $h^2\Omega_{sw}$ and $h^2\Omega_{turb}$ decrease with parameter α . This means that hyperscaling violation θ enhances the energy densities of the sound wave spectrum $h^2\Omega_{sw}$ and the MHD turbulence spectrum $h^2\Omega_{turb}$. From Figure 3d, it is found that the GW spectrum of bubble collision $h^2\Omega_{env}$ coincides with the total GW spectrum $h^2\Omega(f)$. This indicates that the total GW spectrum is dominated by the contribution of the bubble collision in case of runaway bubbles.

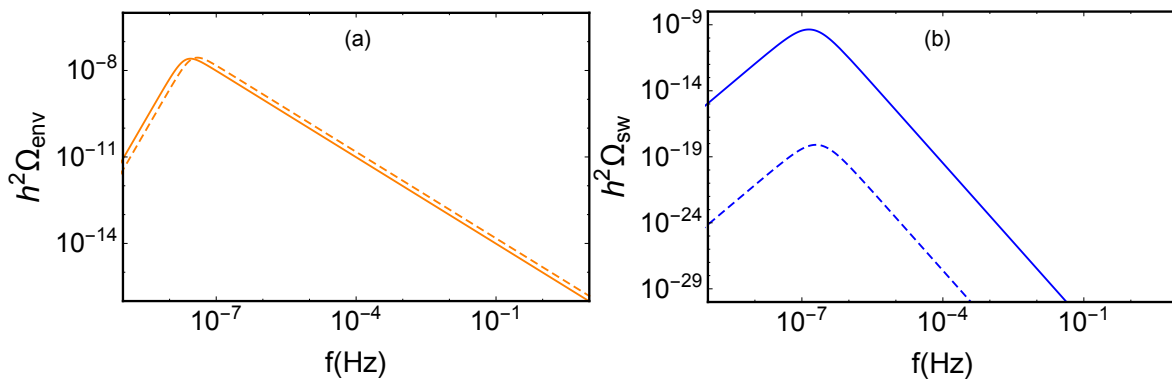


Figure 3. Cont.

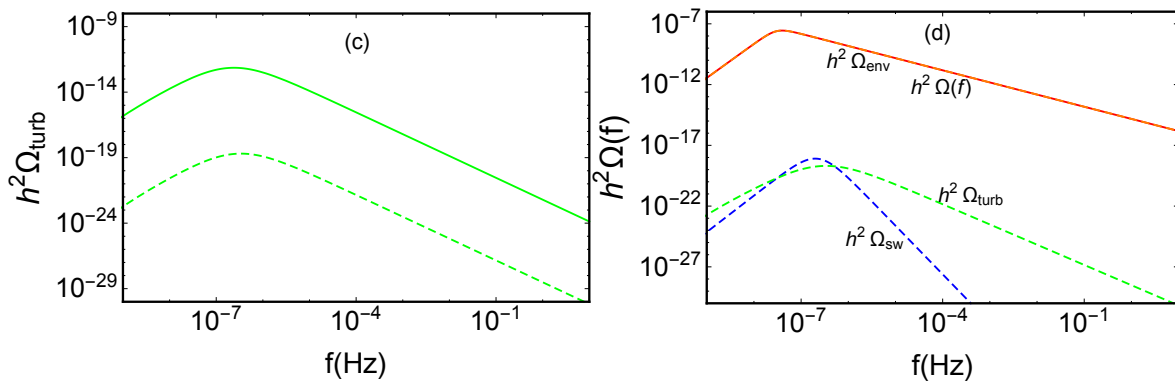


Figure 3. The effects of hyperscaling violation on $h^2\Omega_{env}$, $h^2\Omega_{sw}$, and $h^2\Omega_{turb}$ are plotted in (a–c) respectively, where the solid lines (dashed lines) denote $\alpha = 0.01$ ($\alpha = 0.7$). The GWs spectrum of $h^2\Omega(f)$, $h^2\Omega_{env}$, $h^2\Omega_{sw}$, and $h^2\Omega_{turb}$ when $\alpha = 0.7$ is plotted in (d). The solid red line represents $h^2\Omega(f)$. The dashed orange, dashed blue, and dashed green lines denote $h^2\Omega_{env}$, $h^2\Omega_{sw}$, and $h^2\Omega_{turb}$ respectively.

4. Conclusions and Discussion

Cosmological confinement–deconfinement QCD phase transition can be seen as a source of the GWs. Exploring QCD phase transition helps us comprehend how different phases emerged during its early stages.

In this paper, we consider an Einstein–Maxwell dilaton background and discuss the confinement–deconfinement phase transition between thermally charged AdS and AdS black holes. It is found that chemical potential and hyperscaling violation reduce the phase transition temperature. In a further study, we study the effect of hyperscaling violation on the GW spectrum. It is found that the position of peak frequency moves backward when the hyperscaling violation exponent increases. This means that the hyperscaling violation exponent suppresses the peak frequency. Moreover, the results of the GW spectrum can be detected by IPTA, SKA, and BBO. The GW spectrum may be detected by NANOGrav when there are large hyperscaling violations. The GW signals cannot be probed by TianQin and Taiji temporarily.

We also discuss the effect of hyperscaling violation on the spectrum of bubbles collision, sound waves, and magnetohydrodynamic turbulence. We found that hyperscaling violation θ suppresses the peak frequency of $h^2\Omega_{env}$. Hyperscaling violation enhances the energy densities of the sound wave spectrum $h^2\Omega_{sw}$ and the MHD turbulence spectrum $h^2\Omega_{turb}$. Moreover, the total GW spectrum is dominated by the contribution of the bubble collision in the case of runaway bubbles.

We hope that this work gives some theoretical reference for investigating the early universe. It would also be meaningful to study the GWs of phase transition with nonzero magnetic field. We leave this work for the future.

Author Contributions: Conceptualization, Z.Z.; Formal analysis, Z.Z. and M.S.; Investigation, Z.Z. and M.S.; Writing—original draft, R.Z. and J.H.; Writing—review and editing, D.H. All authors have read and agreed to the published version of the manuscript.

Funding: Defu Hou is supported by the National Natural Science Foundation of China under Grant No. 12275104. Defu Hou is also supported in part by the National Key Research and Development Program of China under Contract No. 2022YFA1604900. Manman Sun is supported by the National Natural Science Foundation of China under Grant No. 12305076. Rui Zhou is supported by the Science and Technology Development Plan Project of Henan Province No. 242102230085.

Data Availability Statement: Data are contained within the article.

Conflicts of Interest: The authors declare no conflicts of interest.

References

1. Einstein, A. Approximative Integration of the Field Equations of Gravitation. *Sitzungsber. Preuss. Akad. Wiss. Berl. (Math. Phys.)* **1916**, *1916*, 688–696.
2. Einstein, A. Uber Gravitationswellen. *Sitzungsber. Preuss. Akad. Wiss. Berl. (Math. Phys.)* **1918**, *1918*, 154–167.
3. Abbott, B.P. et al. [LIGO Scientific and Virgo] Observation of Gravitational Waves from a Binary Black Hole Merger. *Phys. Rev. Lett.* **2016**, *116*, 061102. [[CrossRef](#)] [[PubMed](#)]
4. Arzoumanian, Z. et al. [NANOGrav] The NANOGrav 12.5 yr Data Set: Search for an Isotropic Stochastic Gravitational-wave Background. *Astrophys. J. Lett.* **2020**, *905*, L34. [[CrossRef](#)]
5. Cai, R.G.; Cao, Z.; Guo, Z.K.; Wang, S.J.; Yang, T. The Gravitational-Wave Physics. *Natl. Sci. Rev.* **2017**, *4*, 687–706. [[CrossRef](#)]
6. Kosowsky, A.; Turner, M.S.; Watkins, R. Gravitational waves from first order cosmological phase transitions. *Phys. Rev. Lett.* **1992**, *69*, 2026–2029. [[CrossRef](#)] [[PubMed](#)]
7. Kosowsky, A.; Turner, M.S. Gravitational radiation from colliding vacuum bubbles: Envelope approximation to many bubble collisions. *Phys. Rev. D* **1993**, *47*, 4372–4391. [[CrossRef](#)]
8. Kamionkowski, M.; Kosowsky, A.; Turner, M.S. Gravitational radiation from first order phase transitions. *Phys. Rev. D* **1994**, *49*, 2837–2851. [[CrossRef](#)]
9. Caprini, C.; Hindmarsh, M.; Huber, S.; Konstandin, T.; Kozaczuk, J.; Nardini, G.; No, J.M.; Petiteau, A.; Schwaller, P.; Servant, G.; et al. Science with the space-based interferometer eLISA. II: Gravitational waves from cosmological phase transitions. *JCAP* **2016**, *4*, 1. [[CrossRef](#)]
10. Jinno, R.; Nakayama, K.; Takimoto, M. Gravitational waves from the first order phase transition of the Higgs field at high energy scales. *Phys. Rev. D* **2016**, *93*, 045024. [[CrossRef](#)]
11. Gao, F.; Sun, S.; White, G. A first-order deconfinement phase transition in the early universe and gravitational waves. *arXiv* **2024**, arXiv:2405.00490.
12. Caprini, C. et al. [LISA Cosmology Working Group] Gravitational waves from first-order phase transitions in LISA: Reconstruction pipeline and physics interpretation. *arXiv* **2024**, arXiv:2403.03723.
13. Han, X.; Shao, G. Stochastic gravitational waves produced by the first-order QCD phase transition. *arXiv* **2023**, arXiv:2312.00571.
14. Arsene, I. et al. [BRAHMS Collaboration] Quark gluon plasma and color glass condensate at RHIC? The Perspective from the BRAHMS experiment. *Nucl. Phys. A* **2005**, *757*, 1. [[CrossRef](#)]
15. Adcox, K. et al. [PHENIX Collaboration] Formation of dense partonic matter in relativistic nucleus-nucleus collisions at RHIC: Experimental evaluation by the PHENIX collaboration. *Nucl. Phys. A* **2005**, *757*, 184. [[CrossRef](#)]
16. Back, B.B. et al. [PHOBOS Collaboration] The PHOBOS perspective on discoveries at RHIC. *Nucl. Phys. A* **2005**, *757*, 28. [[CrossRef](#)]
17. Lucini, B.; Rago, A.; Rinaldi, E. $SU(N_c)$ gauge theories at deconfinement. *Phys. Lett. B* **2012**, *712*, 279–283. [[CrossRef](#)]
18. Aoki, Y.; Fodor, Z.; Katz, S.D.; Szabo, K.K. The QCD transition temperature: Results with physical masses in the continuum limit. *Phys. Lett. B* **2006**, *643*, 46–54. [[CrossRef](#)]
19. Bazavov, A.; Bhattacharya, T.; Cheng, M.; DeTar, C.; Ding, H.T.; Gottlieb, S.; Gupta, R.; Hegde, P.; Heller, U.M.; Karsch, F.; et al. The chiral and deconfinement aspects of the QCD transition. *Phys. Rev. D* **2012**, *85*, 054503. [[CrossRef](#)]
20. Bhattacharya, T.; Buchoff, M.I.; Christ, N.H.; Ding, H.T.; Gupta, R.; Jung, C.; Karsch, F.; Lin, Z.; Mawhinney, R.D.; McGlynn, G.; et al. QCD Phase Transition with Chiral Quarks and Physical Quark Masses. *Phys. Rev. Lett.* **2014**, *113*, 082001. [[CrossRef](#)]
21. Witten, E. Anti-de Sitter space and holography. *Adv. Theor. Math. Phys.* **1998**, *2*, 253. [[CrossRef](#)]
22. Gubser, S.S.; Klebanov, I.R.; Polyakov, A.M. Gauge theory correlators from noncritical string theory. *Phys. Lett. B* **1998**, *428*, 105. [[CrossRef](#)]
23. Maldacena, J.M. The Large N limit of superconformal field theories and supergravity. *Adv. Theor. Math. Phys.* **1998**, *2*, 231. [[CrossRef](#)]
24. Hawking, S.W.; Page, D.N. Thermodynamics of Black Holes in anti-De Sitter Space. *Commun. Math. Phys.* **1983**, *87*, 577. [[CrossRef](#)]
25. Herzog, C.P. A Holographic Prediction of the Deconfinement Temperature. *Phys. Rev. Lett.* **2007**, *98*, 091601. [[CrossRef](#)] [[PubMed](#)]
26. Ahmadvand, M.; Fadafan, K.B. Gravitational waves generated from the cosmological QCD phase transition within AdS/QCD. *Phys. Lett. B* **2017**, *772*, 747–751. [[CrossRef](#)]
27. Ahmadvand, M.; Fadafan, K.B. The cosmic QCD phase transition with dense matter and its gravitational waves from holography. *Phys. Lett. B* **2018**, *779*, 1–8. [[CrossRef](#)]
28. Rezapour, S.; Fadafan, K.B.; Ahmadvand, M. Gravitational waves of a first-order QCD phase transition at finite coupling from holography. *Annals Phys.* **2022**, *437*, 168731. [[CrossRef](#)]
29. Rezapour, S.; Fadafan, K.B.; Ahmadvand, M. Gravitational waves of the QCD phase transition in a 5D soft wall model with Gauss-Bonnet correction. *Phys. Scripta* **2022**, *97*, 035301. [[CrossRef](#)]
30. Chen, Y.; Huang, M.; Yan, Q.S. Gravitational waves from QCD and electroweak phase transitions. *J. High Energy Phys.* **2018**, *5*, 178. [[CrossRef](#)]
31. Ares, F.R.; Hindmarsh, M.; Hoyos, C.; Jokela, N. Gravitational waves from a holographic phase transition. *J. High Energy Phys.* **2020**, *21*, 100. [[CrossRef](#)]
32. Cai, R.G.; He, S.; Li, L.; Wang, Y.X. Probing QCD critical point and induced gravitational wave by black hole physics. *Phys. Rev. D* **2022**, *106*, L121902. [[CrossRef](#)]

33. He, S.; Li, L.; Li, Z.; Wang, S.J. Gravitational Waves and Primordial Black Hole Productions from Gluodynamics by Holography. *Sci. China Phys. Mech. Astron.* **2024**, *67*, 240411. [[CrossRef](#)]
34. Zhu, Z.R.; Chen, J.; Hou, D. Gravitational waves from holographic QCD phase transition with gluon condensate. *Eur. Phys. J. A* **2022**, *58*, 104. [[CrossRef](#)]
35. Batell, B.; Ghalsasi, A.; Low, M.; Rai, M. Gravitational Waves from Naturalness. *J. High Energy Phys.* **2024**, *1*, 148. [[CrossRef](#)]
36. Gouttenoire, Y. Primordial Black Holes from Conformal Higgs. *arXiv* **2023**, arXiv:2311.13640.
37. Kachru, S.; Liu, X.; Mulligan, M. Gravity duals of Lifshitz-like fixed points. *Phys. Rev. D* **2008**, *78*, 106005. [[CrossRef](#)]
38. Koroteev, P.; Libanov, M. On Existence of Self-Tuning Solutions in Static Braneworlds without Singularities. *J. High Energy Phys.* **2008**, *2*, 104. [[CrossRef](#)]
39. Charmousis, C.; Gouteraux, B.; Kim, B.S.; Kiritsis, E.; Meyer, R. Effective Holographic Theories for low-temperature condensed matter systems. *JHEP* **2010**, *11*, 151. [[CrossRef](#)]
40. Sachan, S. Study of confinement/deconfinement transition in AdS/QCD with generalized warp factors. *Adv. High Energy Phys.* **2014**, *2014*, 543526. [[CrossRef](#)]
41. Singh, H. Special limits and non-relativistic solutions. *J. High Energy Phys.* **2010**, *12*, 61. [[CrossRef](#)]
42. Narayan, K. On Lifshitz scaling and hyperscaling violation in string theory. *Phys. Rev. D* **2012**, *85*, 106006. [[CrossRef](#)]
43. Singh, H. Lifshitz/Schrödinger Dp-branes and dynamical exponents. *J. High Energy Phys.* **2012**, *7*, 82. [[CrossRef](#)]
44. Alishahiha, M.; Colgain, E.O.; Yavartanoo, H. Charged Black Branes with Hyperscaling Violating Factor. *J. High Energy Phys.* **2012**, *11*, 137. [[CrossRef](#)]
45. Moore, C.J.; Cole, R.H.; Berry, C.P.L. Gravitational-wave sensitivity curves. *Class. Quant. Grav.* **2015**, *32*, 015014. [[CrossRef](#)]
46. Schmitz, K. New Sensitivity Curves for Gravitational-Wave Signals from Cosmological Phase Transitions. *J. High Energy Phys.* **2021**, *1*, 97. [[CrossRef](#)]
47. Ruan, W.H.; Guo, Z.K.; Cai, R.G.; Zhang, Y.Z. Taiji program: Gravitational-wave sources. *Int. J. Mod. Phys. A* **2020**, *35*, 2050075. [[CrossRef](#)]
48. Sin, S.J. Gravity back-reaction to the baryon density for bulk filling branes. *J. High Energy Phys.* **2007**, *10*, 78. [[CrossRef](#)]
49. Lee, B.H.; Park, C.; Sin, S.J. A Dual Geometry of the Hadron in Dense Matter. *J. High Energy Phys.* **2009**, *7*, 87. [[CrossRef](#)]
50. Hindmarsh, M.; Huber, S.J.; Rummukainen, K.; Weir, D.J. Numerical simulations of acoustically generated gravitational waves at a first order phase transition. *Phys. Rev. D* **2015**, *92*, 123009. [[CrossRef](#)]
51. Jovanovic, V.B.; Ignjatovic, S.R.; Borika, D.; Jovanovic, P. Constituent quark masses obtained from hadron masses with contributions of Fermi-Breit and Glazman-Riska hyperfine interactions. *Phys. Rev. D* **2010**, *82*, 117501. [[CrossRef](#)]
52. Bodeker, D.; Moore, G.D. Can electroweak bubble walls run away? *J. Cosmol. Astropart. Phys.* **2009**, *5*, 9. [[CrossRef](#)]

Disclaimer/Publisher's Note: The statements, opinions and data contained in all publications are solely those of the individual author(s) and contributor(s) and not of MDPI and/or the editor(s). MDPI and/or the editor(s) disclaim responsibility for any injury to people or property resulting from any ideas, methods, instructions or products referred to in the content.